Kelvin-Helmholtz instability and induced magnetic reconnection at the Earth's magnetopause: a 3D simulation based on satellite data

Matteo Faganello, M Sisti, F Califano, B Lavraud

Kelvin-Helmholtz instability and induced magnetic reconnection at the Earth's magnetopause: 3D simulation based on satellite data

M. Faganello[1], M. Sisti[1,2], F. Califano[2] and B. Lavraud[3]

[1] Aix-Marseille University, CNRS, PIIM UMR 7345, Marseille, France
[2] Phys. Dept., University of Pisa, Pisa, Italy
[3] University of Bordeaux, CNRS, LAB UMR 5804, Bordeaux, France

E-mail: matteo.faganello@univ-amu.fr

Abstract.
A 3D two-fluid simulation, using plasma parameters as measured by MMS on September 8th 2015, shows the nonlinear development of the Kelvin-Helmholtz instability at the Earth's magnetopause. It shows an extremely rich dynamics, including the development of a complex magnetic topology, vortex merging and secondary instabilities. Vortex induced and mid-latitude magnetic reconnection coexist and produce an asymmetric distribution of magnetic reconnection events. Off-equator reconnection exhibits a predominance of events in the southern hemisphere during the early nonlinear phase, as observed by satellites at the dayside magnetopause. The late nonlinear phase shows the development of vortex pairing for all latitudes while secondary Kelvin-Helmholtz instability develops only in the northern hemisphere leading to an enhancement of the occurrence of off-equator reconnection there. Since vortices move tailward while evolving, this suggests that reconnection events in the northern hemisphere should dominate at the nightside magnetopause.

PACS numbers: 94.30.cp, 52.35.Vd, 52.65.Kj, 52.35.Mw, 94.30.-d

1. Introduction and aims

The Kelvin-Helmholtz instability (KHI) is a powerful driver for the plasma dynamics at magnetized frontiers, such as the Earth's magnetopause. In particular along the flanks, where a velocity shear exists between the shocked solar wind (SW) and the nearly stagnant magnetospheric plasma, this instability is able to convert the kinetic energy of the SW into magnetic energy, that is finally released via magnetic reconnection. This is possible since the instability develops as a large-scale mode, as compared to the ion skin depth and gyroradius, and behaves as an ideal magnetohydrodynamic (MHD) one. As a consequence, field lines are frozen in the plasma motion and are thus stretched and distorted by the growing instability. Eventually, field line stretching leads to the formation of strong magnetic inhomogeneities, i.e. small-scale current layers where magnetic reconnection can develop (for an overview, see [1, 2] and references therein). Notably, also reconnection can create the conditions for KHI, as when the reconnection outflows turn out to be KH unstable[3] and generate small-scale vortices. These vortices could play the role of seeds for electron-scale reconnection and finally generate plasmoids in elongated, thin current sheets[4, 5, 6].

The occurrence of magnetic reconnection completely changes the transport properties of the frontier separating the two different plasmas. Before reconnection, field lines are parallel to the frontier on both sides of it, like in *tangential discontinuities*. In this configuration, only cross-field transport could mix up the two different plasmas, but neither collisions nor wave-induced transport seem to be able to account for the observed transport[7]. As reconnection proceeds, it is able to modify the global magnetic topology and to create field lines that cross the frontier, generating an *open* magnetopause, and connecting the two different plasmas. Because particles can easily stream along field lines, the mixing between the SW and the magnetospheric plasma is finally boosted.

There are several ways by which the KHI can induce reconnection to occur, depending on the relative orientation of the velocity field and of the magnetic field. When dealing with a three-dimensional (3D) dynamics, and considering northward periods (when the dominant component of the interplanetary magnetic field, advected by the SW, is parallel to the Earth's dipole axis), the most important ones are Type I Vortex Induced Reconnection (VIR)[8, 9] and Mid-latitude reconnection (MLR)[10]. The mechanisms behind these two processes are quite different. Type I VIR relies on the fact that the magnetopause is a large-scale current layer, even before the development of the KHI. Indeed, as soon as the SW and magnetospheric field are not perfectly aligned at low-latitude, the magnetic rotation across the magnetopause is associated to a current density there. In the early nonlinear phase, the velocity field perturbations associated to the growing KHI is able to pinch this original current layer in between vortices and, when its thickness has reached a sufficiently small scale, to force reconnection to occur[8]. Worth noticing, the reconnection rate of Type I VIR is independent of the peculiar physical effect that breaks the frozen-in condition at small scales. This rate is imposed by the growing, ideal MHD KHI and can be higher than the "Fast reconnection" rate for spontaneous reconnection[9].

It is important to note that having a small-scale current layer is only one of the conditions required for reconnection. In the absence of magnetic nulls, as at the low-latitude magnetopause during northward periods, it needs magnetic perturbations with a component perpendicular to the magnetopause and with a wavevector $\mathbf{k}$ perpendicular to the unperturbed magnetic field $\mathbf{B}$ somewhere inside the current layer. The component of $\mathbf{B}$ along $\mathbf{k}$, inverting its direction across the null line $\mathbf{k}\cdot\mathbf{B} = 0$, is the reconnecting field, the one that will undergo reconnection. The other component of $\mathbf{B}$, perpendicular to $\mathbf{k}$, is the so called guide field. This condition is naturally satisfied by the perturbations generated by the KHI, since it develops as a flute mode. In fact, the magnetic tension, proportional to $\mathbf{k}\cdot\mathbf{B}$, reduces the KHI growth rate. When the Alfvén Mach number $M_A = \frac{\Delta U}{|\mathbf{B}|^2/4\pi m_i n}$ is of order one and the velocity field and $\mathbf{B}$ are roughly perpendicular, the dominant KHI mode (the one that is the fastest to grow) emerges with $\mathbf{k}\cdot\mathbf{B} = 0$ at, more or less, the center of the layer[11, 12]. The dominant mode "prefers" minimizing the damping action of the magnetic tension instead of maximizing the feeding term given by the velocity inhomogeneity, proportional to $\mathbf{k}\cdot\Delta U$. Here m_i, n and ΔU are the ion mass and number density, and the velocity jump across the layer. Note that $\mathbf{k}\cdot\mathbf{B}$ can not be zero everywhere, since $\mathbf{B}$ rotates across the layer, and that $|\mathbf{k}\cdot\mathbf{B}|$ increases as soon as we move far away from the center of the layer. A cartoon of this configuration is shown in Fig.1, panel a). Clearly, for this orientation of $\mathbf{k}$, the configuration in the dynamical plane defined by the x-direction perpendicular to the unperturbed magnetopause and by the k-direction, is favourable for both KHI and magnetic reconnection, with a null line for the antiparallel in-plane

magnetic field (where $\mathbf{k} \cdot \mathbf{B} = 0$), a guide field and a velocity shear.

The second mechanism, MLR, can act even if the unperturbed magnetopause has no initial current. Starting from a configuration with parallel magnetospheric and SW magnetic fields, magnetic rotation (and so current layers) is generated at mid-latitudes due to the differential advection of field lines with respect to latitude[10]. Indeed, the high-latitude portions of field lines, in both hemispheres, belong to regions that are stable with respect to the KHI. As a consequence, these portions are advected at the unperturbed magnetospheric or SW velocity. On the contrary, once the low-latitude portions are engulfed in large-scale KH vortices, that develop there, they are advected at the KHI phase velocity (roughly the average velocity between the SW one and the magnetospheric one). The result is that magnetospheric and SW lines are arched in opposite directions, cross at mid-latitudes, leading to the formation of current layers there. Magnetic reconnection can thus proceed at mid-latitudes. In the symmetric case, when the magnetic field is strictly northward on both side of the magnetopause, MLR creates double-reconnected flux tube that are connected to the Earth but are partially populated by SW plasma[10, 13]. Note that MLR is different from Type II VIR, for which reconnection is related to the rolling-up of field lines in a 2D configuration. In particular, even if Type II VIR modifies the magnetic topology, it occurs among lines of the same kind, without connecting different plasmas[14, 15].

The rate of production of double-reconnected flux tube is high enough for explaining the entering of SW particles inside the magnetosphere. At the same time, their production can explain the "specific entropy" increase, just inside the magnetopause, that is observed during northward periods[16]. Regarding the plasma transport, also Type I VIR can account for it. Indeed, the effective diffusion coefficient, associated to the Type I VIR process, is of the same order of magnitude or even higher than the one that is required for explaining the observed mixing[17].

Type I VIR and MLR have been observed during different KH events, with different orientation of the magnetic field[18, 19, 20, 21]. Interestingly, the KH event observed by the MMS mission on September 8th 2015 shows Type I VIR and MLR acting at the same time[22, 23, 24]. The coexistence of these two mechanism, and the field lines dynamics during the early nonlinear phase of KH vortices have been investigated numerically. In particular, it has been elucidated why the latitudinal distribution of off-equator reconnection events exhibits more events in the southern hemisphere than in the northern[25] (here off-equator means far from the equatorial plane where the MMS satellites are, and where the KH vortices are supposed to be more developed). This paper investigates the late nonlinear phase of the KH vortices, that is supposed to occur downstream of the MMS satellite location. At that time, processes such as vortex pairing or secondary hydrodynamic instabilities, developing along the arms of large-scale KH vortices, compete in determining the final evolution[26, 27, 28]. In particular, it shows a complex dynamics, with vortex pairing dominating at all latitudes, while secondary instabilities develop locally, in one of the two hemisphere and force reconnection to occur there, leading to a completely different distribution of reconnection events.

This paper is organized as follows: Sec. 2 presents the starting equilibrium for simulations, the model equations and the code details. Sec.3 and 4 analyses the linear, early and late nonlinear phase of the KHI. Sec.5 investigate the properties of magnetic reconnection in such a system. Sec.6 discusses and resumes the results.

2. Starting equilibrium and model equations

We consider a two-dimensional MHD equilibrium that modelizes the plasma and field conditions at the magnetospheric flanks. Taking a straight magnetopause, $\mathbf{x}$ represents the normal direction, going from the magnetosphere to the SW, $\mathbf{z}$ is the latitude direction. The y-direction is the invariant direction for the equilibrium and is along the SW direction. Being independent of y, all physical quantities are functions of a flux function ψ_{eq}, that must satisfy the Grad-Shafranov equation[29]

$$\nabla^2\psi_{eq} = \frac{d\Pi}{d\psi_{eq}} \quad ; \quad \Pi = P_{eq,th} + \frac{B_{eq,y}^2}{2} \tag{1}$$

where the thermal pressure P_{th} is the sum of the ion and electron contributions, P_i and P_e respectively. A suitable solution for modelling the flank is

$$\psi_{eq} = \frac{2}{3}x + \frac{L_z}{6\pi}\sinh\frac{2\pi x}{L_z}\cos\frac{2\pi z}{L_z} \quad ; \quad \Pi = cst \tag{2}$$

together with

$$\mathbf{B}_{eq} = \nabla\times\psi_{eq}\hat{\mathbf{y}} + \frac{B_{flow}}{2}\left(1+\tanh\frac{\psi_{eq}}{a}\right)\hat{\mathbf{y}} \;\; ; \;\; P_{i,eq} = 4P_{e,eq} \tag{3}$$

$$\mathbf{U}_{eq} = \frac{\Delta U}{2}\left(1+\tanh\frac{\psi_{eq}}{a}\right)\hat{\mathbf{y}} \;\; ; \;\; n_{eq} = 1 + \frac{\Delta n}{2}\left(1+\tanh\frac{\psi_{eq}}{a}\right). \tag{4}$$

All quantities are normalized using m_i, n, the ion charge, the number density, the z-component of the Alfvén velocity and the ion skin depth at the magnetopause, at zero latitude ($x = z = 0$). Setting $x \in [-45, +45]$ and $z \in [-48\pi, +48\pi]$ ($L_z = 96\pi$), together with $a = 3$ and a flow-aligned component in the SW equal to $B_{flow} = -0.3$ (to be compared to $B_{eq,z}|_{x=z=0} = 1$), we get a configuration with a dominant z-component for B_{eq}, that is strictly northward inside the magnetosphere and rotates of an angle $\phi \simeq 20°$ crossing the magnetopause. A sketch of the equilibrium magnetic configuration is shown in Fig. 1, panel b). Because $\mathbf{U}_{eq}$ is constant along field lines, the velocity gradient is larger around $z = 0$ than at high-latitudes, resulting in a KHI growing far slower there and in effective high-latitude stabilization[30].

We set $\Delta n = 1$, $\Delta U = 0.9$ and $(P_{i,eq} + P_{e,eq})|_{\psi=0} = 0.9$. These values have been based on the data from the MMS event of September 8th 2015, as provided in the auxiliary materials of[22]. In particular, a number density passing from $5.7cm^{-3}$ in the outer magnetosphere to $20.1cm^{-3}$ in the adjacent magnetosheath, a velocity jump of about $350Km$, and a temperature varying from $\sim 2800eV$ to $\sim 200eV$. The GSE z-component of the magnetic field is more or less constant at $\sim 67nT$ while the flow-aligned component goes from zero to $-24nT$. We note that the temperature jump in our equilibrium, satisfying the condition 2 correspond to $\sim 2080eV$ in physical units, a bit smaller but consistent with the observed one.

We adopt a quasineutral two-fluid model, whose equations, in conservative form, read

$$\partial_t n + \nabla\cdot(n\mathbf{U}) = 0 \tag{5}$$

$$\partial_t(n\mathbf{U}) + \nabla\cdot\left(n\mathbf{U}\mathbf{U} + \left(P_i + P_e + |\mathbf{B}|^2/2\right)\mathbf{I} - \mathbf{B}\mathbf{B}\right) = 0 \tag{6}$$

$$\partial_t\left(nS_{e/i}\right) + \nabla\cdot\left(nS_{e/i}\mathbf{u}_{e/i}\right) = 0 \quad ; \quad S_{e/i} = n^{-5/3}P_{e/i} \tag{7}$$

$$\partial_t\mathbf{B} = -\nabla\times\mathbf{E} \tag{8}$$

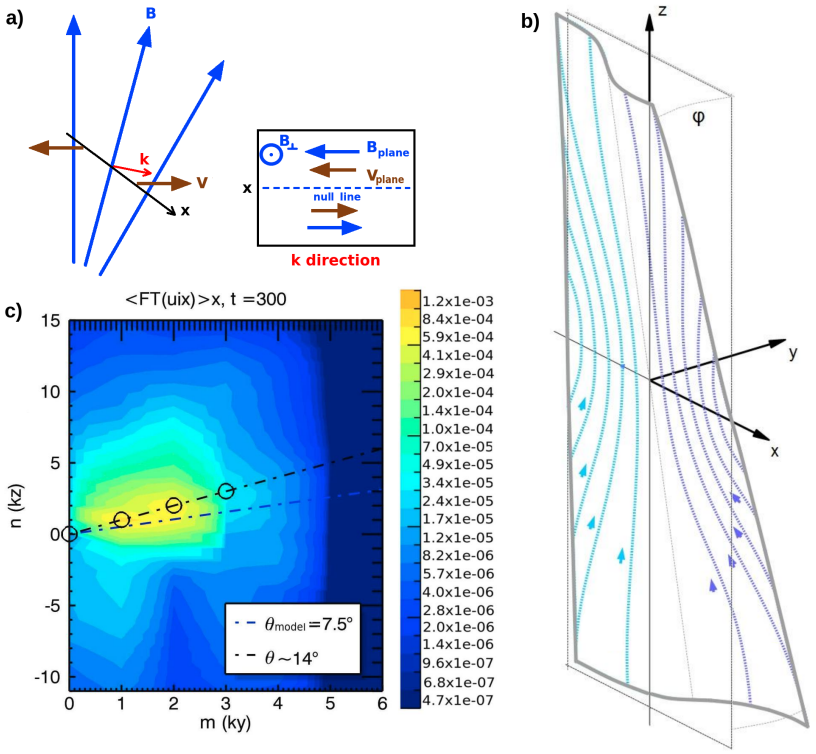

Figure 1. (color online) Panel a): a cartoon of the magnetic and velocity configuration leading to Type I VIR. On its right, its projection on the dynamical plane defined by x- and the wavevector directions. Panel b): a sketch of the equilibrium magnetic configuration adopted in this paper, including high-latitude stabilization. Magnetospheric and SW field lines are drawn in pale and dark blue, respectively. Panel c): magnitude of the x-averaged Fourier coefficients, for m, n-modes of U_x, at $t = 300$. The mode numbers m and n refer to the y and z respectively. The circles underline the position in the (m, n)-plane of the most intense mode, for four different values of m.

The electric field $\mathbf{E}$ is provided by a generalized Ohm's law, neglecting the electron inertia but retaining the Hall and diamagnetic terms, as well as a small but finite resistivity:

$$\mathbf{E} = -\mathbf{u}_e \times \mathbf{B} - \frac{1}{n}\nabla P_e + \eta \mathbf{J} \tag{9}$$

We neglect the displacement current, so that the current density read $\mathbf{J} = \nabla \times \mathbf{B}$, while the ion and electron fluid velocity are given by $\mathbf{u}_i \simeq \mathbf{U}$ and $\mathbf{u}_e = \mathbf{U} - \mathbf{J}/n$ respectively. We note that the resistive diffusion time, associated to the smallest equilibrium length scale a is of the order of 10^4. The dynamics we are interested in happens on a shorter timescale (~ 500). Thus field lines can be considered as frozen in the plasma motion and a modification of their connectivity should be ascribed to magnetic reconnection. Independently of the fact that reconnection is forced, as Type I VIR or develops spontaneously as for MLR, its rate is expected to be independent of η. Indeed, as already discussed, Type I VIR is ruled by the growing ideal KHI[8]. Regarding MLR, it typically develops in current layers whose width is of the order of

the ion skin depth[10]. In that case, the Hall term included in the generalized Ohm's law 9 allows for "Fast reconnection"[31].

The flux function ψ is constant along equilibrium field lines, thus can be seen as a plasma label, with $\psi = 0$ corresponding to the magnetopause, $\psi < 0$ to magnetospheric plasma and $\psi > 0$ to the SW one. We add a fictive evolution equation for ψ, that is simply advected by the plasma velocity as a passive tracer. In such a way, it is possible to follow the ideal evolution of the magnetopause isosurface and to quantify the topological modifications generated by magnetic reconnection. Indeed, in the case of an ideal evolution, ψ would remain constant along field lines. In the actual evolution, where the magnetic field is determined by Eqs.8&9, a variation of ψ along a line would detect the occurrence of magnetic reconnection.

These equations are integrated numerically, using a 4th order Runge-Kutta scheme for time advection, 6th order finite differences for derivatives along $\hat{\mathbf{y}}$ and $\hat{\mathbf{z}}$, and a 6th order implicit compact scheme, with spectral-like resolution, for derivatives along $\hat{\mathbf{x}}$[32].Numerical stability is achieved by means of filters, explicit filters along $\hat{\mathbf{y}}$ and $\hat{\mathbf{z}}$, and a 6th order spectral-like filtering scheme along $\hat{\mathbf{x}}$[32]. At the y and z boundaries, we impose straightforward periodic conditions, while the x-boundaries have more refined conditions based on MHD characteristics [33]. They allow for any magnetosonic or alfvénic fluctuations to simply leave the numerical domain, and permit to sustain the equilibrium configuration that is far from being homogeneous at the boundaries.

The box size along $\hat{\mathbf{y}}$ is set as $L_y = 24\pi$, twice the wavelength of the dominant KH mode, roughly given by $4\pi a$. The number of grid points is $n_x = 600$, $n_y = n_z = 512$.

3. The linear and the early nonlinear evolution

During the linear phase, the KHI grows exponentially, with a growth rate for the dominant mode of about 0.02. The dominant mode has a mode number $m = 2$, as expected by the choice $L_y = 24\pi$. Here m and n are the mode numbers with respect to y and z respectively. The dominant mode does not have a wavevector strictly aligned with the velocity field, but slightly tilted. Fig. 1, panel c), shows the magnitude of m, n-modes, at the end of the linear phase ($t = 300$), averaged over the x-direction. The circles underline the position in the (m, n)-plane of the most intense mode, for four different values of m. They are aligned with a direction indicated by the dot-dashed line, that is rotated by an angle $\theta \sim 14^\circ$ with respect to the horizontal direction. The wavevectors associated to this angle are not perpendicular to the equilibrium magnetic field at the precise center of the layet ($x = 0$) but at its direction at $x \simeq 2$.

The fact that $\mathbf{k}$ is not perpendicular to the magnetic field direction at the precise center of the layer, is due to the fact that, for the present equilibrium, the Alfvén velocity is slightly greater in the SW than in the magnetosphere. The mode thus prefers to develop at an angle in between the magnetic angle at the center of the layer ($\sim 10^\circ$) and the one in the SW ($\sim 20^\circ$). It is worth noting that adopting a simplified linear model, with 1D step-like profiles for n_{eq}, $\mathbf{U}_{eq}$ and $\mathbf{B}_{eq}$, would not reproduce the correct angle for the dominant mode. Indeed, the well-known formula[34, 35, 36] $\gamma^2 = \frac{n_1 n_2}{(n_1+n_2)^2} \left[\mathbf{k} \cdot (\mathbf{U}_2 - \mathbf{U}_1)\right]^2 - \frac{1}{(n_1+n_2)} \left[(\mathbf{k} \cdot \mathbf{B}_1)^2 + (\mathbf{k} \cdot \mathbf{B}_2)^2\right]$ where γ is the linear growth rate and the subscribes 1 and 2 denotes the asymptotic values of our equilibrium configuration, is maximized for $\theta_{model} \sim 7.5^\circ$. The finite width of the shear layer must be taken into account, not only for explaining the

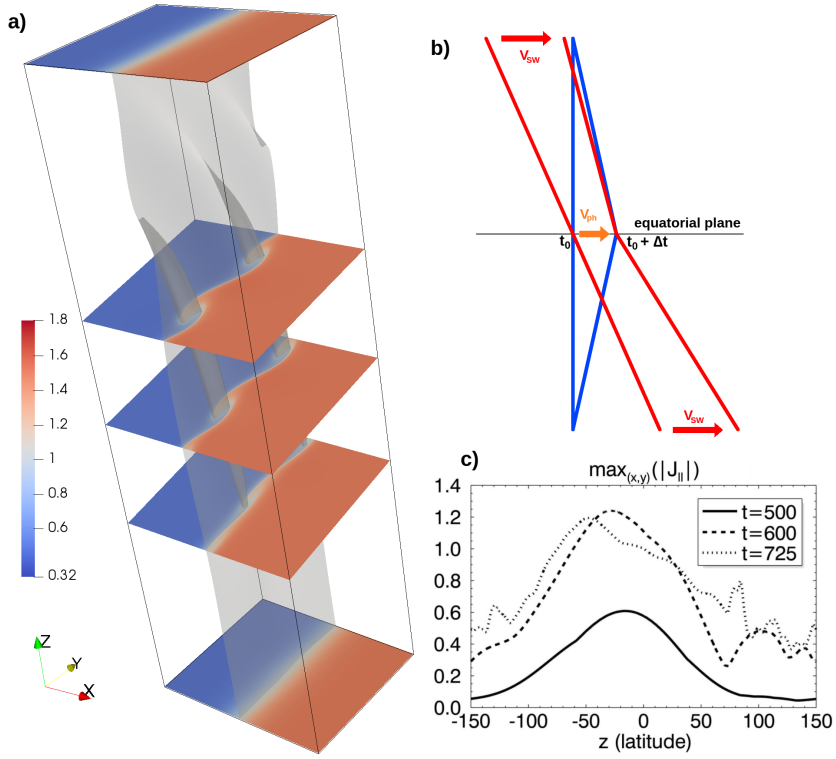

Figure 2. (color online) Panel a): plasma density at $t = 500$. The three central planes are defined by $\hat{\mathbf{x}}$ and the direction of the dominant wavevector (forming an angle of $\sim 14°$ respect to $\hat{\mathbf{y}}$). The shaded $\psi = 0$ isosurface represents the magnetopause. Panel b): a sketch of the differential advection mechanism leading to an increase of magnetic rotation in the norther hemisphere. A magnetospheric (SW) line is represented in blue (red) at t_0 and $t_0 + \Delta t$, in the Earth's rest frame. Panel c): the maximum of $|J_{\|}| = |\mathbf{J} \cdot \mathbf{B}|/|\mathbf{B}|$ for each $z = cst$ plane, as a function of z.

value of the growth rate of the dominant mode[37], but also for the angle at which it develops[11, 38].

In the nonlinear phase, the KHI develops in rolled-up vortices at mid-/low-latitudes while the high-latitude planes stay stable, as shown in Fig.2, panel a), at $t = 500$. As expected, the vortex axis are inclined with respect to the z-direction, as well as the folds of the $\psi = 0$ shaded isosurface, the perturbed magnetopause. The presence of a flow-aligned component of the magnetic field breaks the north-south symmetry of the system, and KH vortices develop asymmetrically with respect to the equatorial plane. In fact, when the pseudoscalar defined by $\mathbf{\Omega}_{eq} \cdot \mathbf{J}_{eq}$ is negative, as in the present case, vortices are expected to develop preferentially in the northern hemisphere[39], as they do. Here $\mathbf{\Omega}_{eq}$ and $\mathbf{J}_{eq}$ are the vorticity and current density of the equilibrium configuration, at the center of the layer. This behaviour can be explained by how field lines, still frozen in the fluid motion, are advected at different latitudes. At high-latitude, where the plasma flow stays quiet, magnetospheric and SW field lines are advected at the unperturbed magnetospheric and SW velocities, respectively. At low-latitude, as soon as field lines are caught by vortices, they are

advected at the KH phase velocity, approximatively the average of the velocities of the two regions. Fig.2, panel b), shows a sketch of this mechanism and how the magnetic rotation in the northern and in the southern hemisphere is modified differently when a couple of field lines at time $t = t_0$ is advected by the plasma velocity for an interval Δt. For the sake of simplicity, the sketch is drawn in the Earth's rest frame. Since magnetic rotation, that is enhanced in the southern hemisphere, stabilizes the KHI, vortices gradually shifts in the northern hemisphere.

A more quantitative measure of the evolution of magnetic rotation is provided by the current density. Fig.2, panel c), shows the temporal evolution of the maximum value of $|J_{\|}| = |\mathbf{J} \cdot \mathbf{B}|/|\mathbf{B}|$ for each $z = cst$ plane, as a function of z. As time goes on, up to $t = 600$, the current maximum grows, due to the current pinching in between vortices, the mechanism that underlies Type I VIR. This growth is enhanced in the southern hemisphere, and reduced in the northern one, by the differential advection of field lines.

4. Pairing and secondary instabilities in the late nonlinear phase

In the late nonlinear phase, two different hydrodynamic phenomena compete: vortex pairing[26] and vortex disruption due to the development of small-scale, secondary KH and Rayleigh-Taylor instabilities along the rolled-up arms of the vortices. The local velocity and density inhomogeneities, as well as the effective gravity, necessary for the development of secondary instabilities, are enhanced when the initial density jump across the magnetopause is larger[27]. The larger the jump, the higher the probability that secondary instability disrupt vortices before they can merge and form larger and larger structures[28, 40]. In 2D simulations, the "in-plane" magnetic field seems to partially stabilizes secondary instabilities, and thus to favour the pairing process[41, 42], since the magnetic tension is more efficient at smaller scales. In 3D simulations, neglecting high-latitude stabilization, this stabilization is less efficient: secondary instabilities can develop with a wavevector perpendicular to the local magnetic field, reducing the importance of the magnetic tension. As a consequence, they seem to dominate the evolution, disrupt the vortices and create a mixing-layer[17]. When the high-latitude stabilization is taken into account, its impact is twofold. On the one hand, the pairing process is stopped as soon as the wavelength ($\sim$ along $\hat{\mathbf{y}}$) of the vortices is comparable with the height of the unstable region, the region in between two high-latitude stable regions[43]. On the other hand, the curvature of magnetic field lines during the 3D evolution of the primary KHI could stabilize secondary instabilities, in particular if the local direction of the magnetic field varies on a length scale comparable to the wavelength of secondary instabilities. The higher the unstable zone, the smaller, in principle, the magnetic curvature.

The present simulation, based on the magnetopause parameters of September 8th 2015, takes all these mechanisms into account, with a height of the unstable region that is ~ 4 times greater than the wavelength of the primary KHI. As a consequence, from $t = 525$ to $t = 650$, the two vortices interact and finally merge, as shown in Fig.3, left panel. During this process, any secondary instability develops. On the contrary, secondary instabilities develop quite quickly, as compared to the time interval required for vortex merging, in the northern hemisphere, along the external boundary of the left arm of the vortex, the one filled by SW plasma, where strong gradients are present. They develop in the latitude region, $20 < z < 90$, where the vortical motion of the vortices is intense enough and, at the same time, the magnetic rotation (current) is

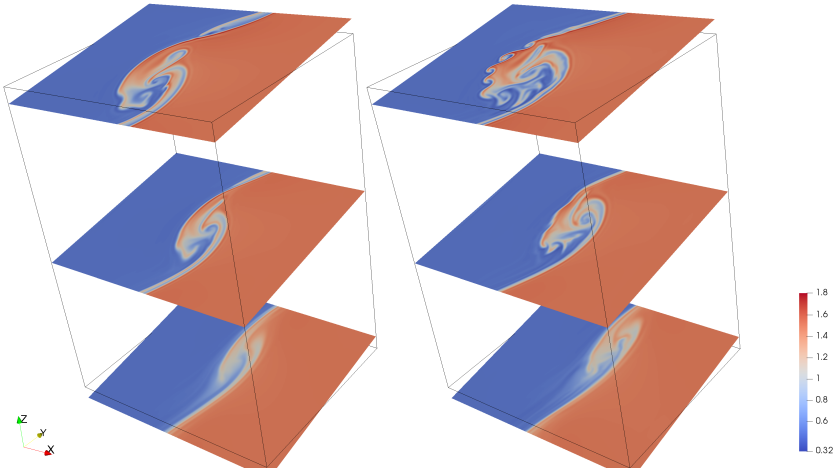

Figure 3. (color online) Left (right) Plasma density at $t = 675$ ($t = 725$). The simulation box is represented only for $-64 < z < 64$, The three planes, centered in $z = -64,\ 0\ 64$, are perpendicular to the vortex axis direction and form an angle of $\sim 9°$ with the y-direction.

low enough. Indeed, magnetic rotation has a stabilizing effect on both primary KH vortices, but also on secondary instabilities.

The pattern of secondary instabilities, as shown in the top plane of Fig.3, right panel, reproduces small-scale vortices and suggests a predominance of secondary KHI over secondary Rayleigh-Taylor instability, that otherwise would generate mushroom-like structures. This predominance is confirmed by a local stability analysis at $t = 675$, just before that the deformations of the vortex boundary are visible, along the external boundary of the left vortex arm, at $z = 64$, where the perturbations will appear more vigorous. The local Richardson number is defined as $Ri = \frac{g_{eff}}{n}\frac{|\partial_i n|}{|\partial_i U_j|^2}$, where $\hat{\mathbf{i}} = \nabla n/|\nabla n|$ is the normal direction of the arm boundary and $\hat{\mathbf{j}}$, along the arm boundary, complete the orthonormal basis in the (x, y)-plane ($\hat{\mathbf{z}}$ is, locally, the invariant direction of secondary instabilities). The effective gravity, associated to the plasma rotation induced by the vortex, reads $g_{eff} = |U_j|^2/R_c$, where the curvature radius R_c is given by the curvature radius of the vortex boundary, $R_c^{-1} = |\hat{\mathbf{j}}\cdot\nabla\hat{\mathbf{j}}|$. Along the boundary, where secondary instabilities develops, $Ri = O(10^{-2})$ confirms the KH nature for the secondary instability. We note also that the parallel Alfvén Mach number $M_{A,\parallel} = \Delta U/V_{A,\parallel} = \Delta U_j/V_{A,j}$ is bigger than 5, allowing for the development of rolled-up vortices[9, 33, 37] (generated in this case by the secondary KHI). Here the velocity jump is across the vortex boundary, the parallel direction is $\hat{\mathbf{j}}$ and, for the sake of simplicity, $V_{A,j}$ is the maximum of the "asymptotic" value of the j-component of $\mathbf{V}_A$, i.e. where n, $\mathbf{U}$ and $\mathbf{B}$ roughly reach a plateau. The $M_{A,\parallel}$ value is estimated taking $\hat{\mathbf{z}}$ as the local, invariant direction.

Actually, this direction forms an angle of about 5° with $\hat{\mathbf{z}}$, as underlined by the folds of the perturbed magnetopause (shaded $\psi = 0$ isosurface) in Fig.4, panel a), that nearly follow the local magnetic field direction. As it was the case for the primary KH vortices, developing with an invariant direction/vortex axis parallel to the local magnetic field minimizes the stabilizing role of magnetic tension for the secondary

instability too. Projecting **U** and **B** on the plane perpendicular to this direction, we obtain a $M_{A,\parallel}$ value even greater. In particular, the projection of $B_j\hat{\mathbf{j}}$, on that plane, passes from 0.1 to -0.15 across the current layer. The length of the secondary vortices, along $\hat{\mathbf{y}}$ is ~ 7, about $6-7$ time the width of the local velocity shear before the instability development, as expected for the dominant KH mode.

5. Induced magnetic reconnection

The reconnection dynamics of Type I VIR and MLR of this KH events has been largely investigated in Ref.[25]. Here we resume the main points regarding Type I VIR and MLR in the early linear phase and finally focus on the late nonlinear phase. During the early nonlinear phase, as the current is enhanced around $z = 0$, magnetic reconnection is favoured there. Even if the KH wavevector is not perpendicular to the magnetic field direction at the precise center of the current layer, the condition $\mathbf{k}\cdot\mathbf{B}_{eq}$ is satisfied at $x \simeq \psi \simeq 2$, given $\theta \simeq 14°$, a position where the equilibrium current density is $\sim 60\%$ of its maximum value. As a consequence, Type I VIR is expected to occur, forced by the growing KHI. Later, a second, smaller current peak is created by differential advection in the northern hemisphere, as shown in Fig.2, panel c), at $t = 600$. Indeed, after having reduced the magnetic angle to zero, differential advection continues to rotates field lines, creating currents with an opposite direction ($J_z > 0$) with respect to the original one ($J_z < 0$). Both local current layers, the one whose current peak is close to the equatorial plane and that having a current maximum in the northern hemisphere, are located in between vortices and have a width of the order of the ion skin depth.

These current layers are characterized by a guide field, given by **B** at the local maximum of $|J_\parallel|$, and an in-plane reconnecting field perpendicular to it. At $t = 600$, the in-plane field inverts its direction across the current layer, with a magnitude, close to the layer, of $+0.4$ for $z \sim -30$, and of 0.2 for $z \sim 100$. Clear signatures (ion/electron outflows, Hall quadrupole) of reconnection are visible in both current layer, as shown in the "Supporting Information"[44] of Ref.[25]. Nevertheless, as time goes on, vortex merging and the development of secondary KH vortices render the 3D configuration quite complex. Finding reconnection signatures becomes a hard task. For this reason, we directly look at the topological properties of magnetic field lines.

For detecting reconnected lines, 22500 field lines are integrated, for each time, starting from uniformly distributed feet at $z = -48\pi$, $x \in [-15, 15]$, $y \in [0, 24\pi]$. We define a line as reconnected if it crosses the magnetopause ($\psi = 0$) and connects the magnetospheric and SW plasmas ($\psi < -a/4$ and $\psi > +a/4$, respectively). The line is classified as *once-reconnected*, *twice-reconnected*, etc., depending on the number of magnetopause crossings, respecting the threshold condition on the ψ-jump. The orientation of **k** during the linear phase would suggest that Type I VIR should occur at $\psi \simeq 2$. Nevertheless, we have chosen to consider jumps across $\psi = 0$ because i) the $\psi = 0$ isosurface represents the perturbed magnetopause and ii) the nonlinear evolution lowers the inclination of the vortex axis with respect to $\theta \simeq 14°$, and modifies the current layer structure. Thus, looking at lines crossing the magnetopause seems to be more representative. For each line, we record the value (or multiple values) of the magnetopause crossing, and thus at which latitude reconnection has developped.

Fig.4, panel b), shows the temporal evolution of magnetopause crossings in the northern and in the southern hemisphere. As showed in Ref.[25], up to $t = 550$, only *once-reconnected* lines appear. All these lines have been created by Type I VIR close to

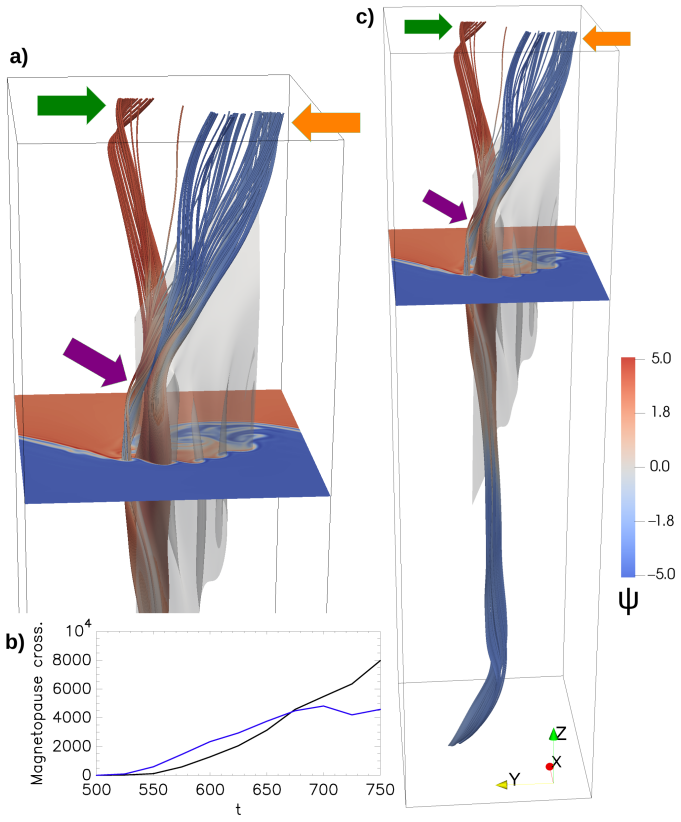

Figure 4. (color online) Panel a): a zoom on the upper part of panel c). Panel b): the temporal evolution of the number of magnetopause crossing of reconnected lines, in the northern hemisphere (black line) and in the southern one (blue line). Panel c): a selection of magnetic field lines, colored according to the ψ-value along the lines. The plane at $z = 64$ show the plasma density, using the same colorbar of Fig.3. Only part of the shaded magnetopause has been drawn. Three arrows indicate bunches of lines with different topologies.

the equatorial plane, or just below, where the main current peak is. Indeed panel b) shows more magnetopause crossing in the southern hemisphere than in the northern. Later, part of these lines reconnect a second time in the northern hemisphere, around $z \simeq 100$, where MLR sets on in the second current peak at $z \sim 100$, as shown by Fig.2, panel c), $t = 600$, creating *twice-reconnected* lines [25]. Notably, in the early nonlinear phase (before the pairing process starts), the number of magnetopause crossing is larger in the southern hemisphere than in the northern one. The same behaviour is observed for "reconnection events", that can be defined as the temporal increment of magnetopause crossing. The reason is that, even if MLR occurs in the norther hemisphere, the dominant Type I VIR gradually shifts southward from the equatorial plane, as the main current peak does. This is in agreement with off-latitude reconnection signatures detected by MMS on September 8th 2015[22, 23, 24], when the KH vortices was observed in the dayside magnetopause, thus in their early nonlinear phase. For the detailed analysis of the latitude distribution of reconnection events, please refer to Ref.[25].

This behaviour is different in the late nonlinear phase. Indeed, reconnection continues during the vortex merging, but slows down, in both the northern and southern hemispheres, when a single, larger-scale vortex is formed ($t = 675$). At $t = 725$, when secondary, small-scale, KH vortices has been formed, reconnection speeds up again, in particular at intermediate latitudes, $20 < z < 90$ [25], as shown in panel b) by the strong increase of magnetopause crossing in the northern hemisphere. In fact, reconnection is forced to occur in between secondary KH vortices, that develops there, following the same Type I VIR mechanism we have discussed about the primary KHI. The current density in between secondary vortices passes from $|\mathbf{J}| = 0.27$ before their formation, to $|\mathbf{J}| = 0.59$ after their development. As a consequence, the number of reconnected lines increases, and lines reconnected more than two times appear. Fig.4, panel a) and c), shows a selection of reconnected lines. Each line is colored using the value of ψ along the line (blue: magnetospheric plasma; red: SW plasma). All lines have been reconnected around the equatorial plane, by Type I VIR in the main current peak, connecting the blue plasma in the southern hemisphere to the red one in the northern. A bunch of these lines (reaching the northern high-latitude plane on the left, as indicated by the green arrow) remains connected to the red plasma in the whole northern hemisphere. All these lines are *once-reconnected*. Another bunch of lines (reaching the northern high-latitude plane on the extreme right, as indicated by the orange arrow), changes its connectivity from the the red plasma to the blue one, at $z \sim 100$ where MLR has been at play, creating *twice-reconnected* lines. Finally, we recognize a *bouquet* of lines (indicated by the violet arrow), crossing the leftmost, small-scale, secondary vortex, where field lines change their connectivity one or few times while turning around the vortex axis. Reconnection induced by secondary, KH vortices in the northern hemisphere, is thus able to create *twice-* and *more-than-twice* reconnected lines, starting from *once-reconnected* lines that have been generated by Type I VIR close to the equators.

6. Discussion and conclusions

These results have been obtained setting the initial configuration of our simulation on the observational data of September 8th 2015, when MMS satellites provides signatures of KH vortices close to the equatorial plane, in their early nonlinear phase, along the dayside magnetopause[22]. In particular, this event has a dominant northward magnetic field, in both the magnetosphere and the SW and a negative flow-aligned magnetic component in the SW. The MHD equilibrium considered in this work is able to mimic this configuration, including high-latitude stabilization. The simulation reproduces the KHI dynamics at the dusk flank of the magnetosphere, that where satellites are.

From the present results we can infer the properties of the KHI, and induced reconnection, for a positive flow-aligned component of the magnetic field in the SW. Indeed, it is possible to obtain the same initial configuration, but with a positive flow-aligned component of the magnetic field, simply reflecting the system about the equatorial plane (thus sending $z \longrightarrow -z$). Because the two-fluid equations are invariant under this transformation, the KHI and reconnection dynamics will be simply specular with respect to the equatorial plane. This implies that everytime a phenomenon is dominant in one hemisphere (e.g. primary KHI more intense in the northern hemisphere) for a negative flow-aligned component of the SW magnetic field, it would be dominant in the opposite one for a positive flow-aligned component.

Regarding the dawn flank of the magnetosphere, it is possible to obtain its configuration and the dynamics there, reflecting the system about the plane defined by the SW direction and the Earth's dipole axis ($\hat{\mathbf{y}}$ and $\hat{\mathbf{z}}$ in our simulation) and applying charge conjugation. As before, two-fluid equations are invariant with respect to this transformation, so that the dynamics is expected to be specular at the two flanks, e.g. the hemisphere where primary KH vortices are more intense would be the same at both flanks.

The main properties, at both flanks, for a negative (positive) flow-aligned component of the SW magnetic field, can be summarized as follow:

- The KHI develops in rolled-up vortices in a large latitude region across the equatorial plane, where the KH linear growth rate is maximal. Nevertheless, due to the differential advection of magnetic field lines during the early nonlinear evolution, vortices develop more vigorously in the northern (southern) hemisphere.
- Type I VIR, forced by the KHI close to the equatorial plane, is more intense in the southern (northern) hemisphere, since the pinching of the original magnetopause current density is stronger there. At the same time, MLR occurs in the northern (southern) hemisphere. The latitude distribution of off-equator reconnection events (being them related to MLR or to off-equator Type I VIR), during the early nonlinear phase (before vortices start to merge), exhibits a larger number of events in the southern hemisphere, as observed by the MMS satellites for this configuration[22, 23, 24, 25]. For a positive flow-aligned component of the SW magnetic field we expect more events in the northern hemisphere.
- In the late nonlinear phase, vortices merge and create larger and larger vortical structures. This process is observed at all latitudes where original vortices are. At the same time, secondary, small-scale KH vortices develop along the SW arm of primary vortices. These small-scale vortices develop only in the northern (southern), where the primary KHI, feeding them, is more intense while the stabilizing magnetic rotation is low enough.
- Reconnection is forced to occur by small-scale vortices, over a large latitude region of the northern (southern) hemisphere, finally following the same mechanism of Type I VIR but going on locally, far away from the equatorial plane. As a consequence, the number of reconnection events increases locally, and their latitude distribution shows more off-latitude events in the northern (southern) hemisphere. Complex magnetic topologies are observed for field lines crossing these small-scale vortices, including *once-*, *twice-* and *more-than-twice* reconnected lines.

We expect that the late nonlinear dynamics of the KHI and induced reconnection would be detected by satellites located in the nightside magnetopause, downstream of the MMS position on September 8th 2015, as in the real system vortices evolve while moving tailward.

The symmetry properties of our system could be broken either by kinetic effects, in particular by Finite Larmor Radius effects acting differently at the two flanks[45, 46], or by a finite East-West component of the SW magnetic field. In this case, the regions where the KH linear growth rate is maximal shift away from the equatorial plane, in opposite direction at the two flanks[47, 48]. Furthermore, taking into consideration the global dynamics of the whole magnetospheric system, the draping of the East-West

magnetic component around the magnetopause leads to an enhanced flow-aligned component at one flank[49] and thus to different initial configurations for the KHI. Last, passing the bow shock (upstream of the KH development) the SW becomes turbulent at the flank where the shock is quasi-parallel (the East one for a positive East-West component of the SW magnetic field), while it stays more laminar at the opposite flank[50]. The turbulent fluctuations could initiate differently the KHI, with respect to the small amplitude initial perturbations that are usually adopted in numerical simulations. The study of the interaction between the KHI and the SW turbulence remains an open issue.

References

[1] J. R. Johnson, J. R. et al., *Space Sci. Rev.* **184**, 1 (2014).
[2] M. Faganello et al., *J. Plasma Phys.* **83**, 535830601 (2017).
[3] F. Califano et al., *Plasma Phys. Contr. Fus.* **49**, B439 (2007).
[4] R. L. Fermo et al., *Phys. Rev. Lett.* **108**, 255005 (2012).
[5] C. Huang et al., *Geophys. Res. Lett.*, **42**, 7282 (2015).
[6] C. Huang et al., *ApJ* **835**, 245 (2017).
[7] J. Labelle et al., *Space Sci. Rev.* **47**, 175 (1988).
[8] D. A. Knoll et al., *Phys. Rev. Lett.* **88**, 215003 (2002).
[9] T. K. M. Nakamura et al., *Adv. Space. Res.* **37**, 522 (2006).
[10] M. Faganello et al., *Europhys. Lett.* **100**, 69001 (2012).
[11] D. J. Southwood, *Planet. Space Sci.* **16**, 587 (1968).
[12] A. D. M. Walker, *Planet. Space Sci.* **29**, 1119 (1981).
[13] D. Borgogno et al., *Phys. Plasmas* **22**, 032301 (2015).
[14] K. Nykyri et al., *Geophys. Res. Lett.* **28**, 3565 (2001).
[15] T. K. M. Nakamura et al., *Phys. Rev Lett.* **101**, 165002 (2008).
[16] J. R. Johnson et al., *J. Geophys. Res.* **114**, A00D08 (2009).
[17] T. K. M. Nakamura et al., *Geophys. Res. Lett.* **41**, 8704 (2014).
[18] B. Nikutowski et al., *Adv. Space Res.* **29** 1129 (2002).
[19] S. Eriksson, S. et al., *J. Geophys. Res.* **114**, A00C17 (2009).
[20] H. Hasegawa et al., *J. Geophys. Res.* **114**, A12207 (2009).
[21] M. Faganello et al., *Europhys. Lett.* **107**, 19001 (2014).
[22] S. Eriksson et al., *Geophys. Res. Lett.* **43**, 5606 (2016).
[23] Y. Vernisse et al., *J. Geophys. Res.: Space Physics* **121**, 9926 (2016).
[24] Y. Vernisse et al., *J. Geophys. Res.: Space Physics* **125**, e2019JA027333 (2020).
[25] M. Sisti et al., *Geophys. Res. Lett.* **46**, 11597 (2019).
[26] A. Miura, Phys. Plasmas **4**, 2871 (1997).
[27] Y. Matsumoto et al., *Geophys. Res. Lett.* **31**, L02807 (2004).
[28] M. Faganello *et al.*, Phys. Rev. Lett. **100**, 015001 (2008).
[29] T. Andreussi et al., *Phys. Plasmas* **19**, 052102.
[30] M. Faganello et al., *EPS/ICPP 2012, Conf. Proc., Plasma Phys. Control. Fusion special issue* **54**, 124037 (2012).
[31] J. Birn et al., *J. Geophys. Res.*, **106**, 3715 (2001).
[32] S. K. Lele, *J.Comp. Phys.* **103**, 16 (1992).
[33] M. Faganello *et al.*, New J. Phys. **11**, 063008 (2009).
[34] S. Chandrasekhar, Hydrodynamic and hydromagnetic stability, *Oxford University Press* (1961).
[35] W. I. Axford, *Quart. Journ. Mech. and Applied Math.* **8**, 314 (1960).
[36] A. K. Sen, *Phys. Fluids* **6**, 1154 (1963).
[37] A, Miura, *Phys. Rev. Lett.* **19** , 779 (1982).
[38] J. E. Contin, J. E. et al., *J. Geophys. Res.* **108**, 1227 (2003).
[39] S. Fadanelli et al., *J. Geophys. Res.: Space Physics* **123**, 9340 (2018).
[40] M. M. Cowee, M. M. et al., *J. Geophys. Res.* **114**, A10209 (2009).
[41] M. M. Cowee, M. M. et al., *J. Geophys. Res.* **115**, A06214 (2010).
[42] A. Tenerani *et al.*, Plasma Phys. Control. Fusion, **53** 015003 (2011).
[43] K. Takagi *et al.*, J. Geophys. Res. **111** A08202 (2006).
[44] https://agupubs.onlinelibrary.wiley.com/action/downloadSupplement?doi=10.1029%2F2019GL083282&file=grl59652-sup-0001-2019GL083282-Figure_SI-S01.pdf

[45] T. K. M. Nakamura et al., *Phys. Plasmas* **17**, 042119 (2010).
[46] P. Henri et al., *Phys. Plasmas* **20**, 102118 (2013).
[47] C. J. Farrugia et al., *J. Geophys. Res.* **103**, 6703 (1998).
[48] F. T. Gratton et al., *Planet. Space Sci.* **51**, 769 (2003).
[49] K. Nykyri, *J. Geophys. Res.* **118**, 5068 (2013).
[50] A. P. Dimmock et al., *J. Geophys. Res.* **120**, 2767 (2015).